DualCast: A Model to Disentangle Aperiodic Events from Traffic Series

Xinyu Su , **Feng Liu** , **Yanchuan Chang** , **Egemen Tanin** , **Majid Sarvi** and **Jianzhong Qi***
The University of Melbourne
{suxs3@student., feng.liu1@, yanchuan.chang@, etanin@, majid.sarvi@, jianzhong.qi@}unimelb.edu.au

Abstract

Traffic forecasting is crucial for transportation systems optimisation. Current models minimise the *mean* forecasting errors, often favouring periodic events prevalent in the training data, while *overlooking critical aperiodic ones* like traffic incidents. To address this, we propose *DualCast*, a dual-branch framework that disentangles traffic signals into intrinsic spatial-temporal patterns and external environmental contexts, including aperiodic events. DualCast also employs a cross-time attention mechanism to capture high-order spatial-temporal relationships from both periodic and aperiodic patterns. DualCast is versatile. We integrate it with recent traffic forecasting models, consistently reducing their forecasting errors by up to 9.6% on multiple real datasets.

1 Introduction

Traffic forecasting is essential for intelligent transportation systems (ITS), enabling real-time solutions like route planning and transportation scheduling.

Deep learning-based solutions have dominated the traffic forecasting literature in recent years. They typically adopt graph neural networks (GNNs) for modelling spatial patterns and sequential models for modelling temporal patterns [Song *et al.*, 2020; Wang *et al.*, 2020; Li and Zhu, 2021; Fang *et al.*, 2021; Liu *et al.*, 2022; Qi *et al.*, 2022]. Besides, a series of recent studies adopt the attention mechanism to capture dynamic relationships in traffic patterns [Guo *et al.*, 2019; Liu *et al.*, 2023; Tang *et al.*, 2024].

These solutions are primarily designed to minimise *mean* forecasting errors, a common evaluation metric [Xu *et al.*, 2020; Zheng *et al.*, 2020; Jiang *et al.*, 2023a]. This optimisation focuses on *periodic* traffic patterns, which are both easier to forecast and more prevalent in the traffic data, resulting in an easier reduction in mean errors.

These models struggle with rare and random *aperiodic* events, such as traffic incidents, making them difficult to forecast. However, promptly identifying and adapting to such events is essential for effective real-time traffic forecasting.

*Corresponding author.

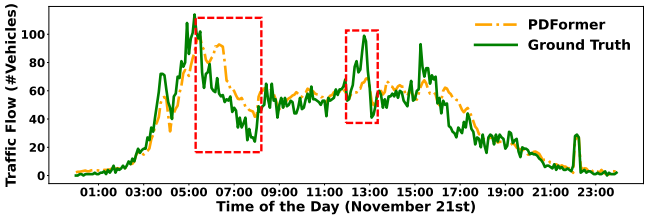

Figure 1: An example of a recent model PDFormer forecasting 60-minute-ahead traffic flows. The model has strong overall results but fails to respond to sudden changes (highlighted by the red boxes).

Fig. 1 shows PDFormer [Jiang *et al.*, 2023a] forecasting the traffic flow on a California freeway 60 minutes ahead for one day (detailed in Section 5.2). There are two substantial gaps between the forecasts (the orange dashed line) and ground truth (the green solid line) at around 07:00 and 13:00. These gaps would be overlooked if only mean forecasting error is considered, as the overall patterns are similar.

In this paper, we propose *DualCast* – a model framework to address the issue above. DualCast is *not* yet another traffic forecasting model. Instead, we aim to present **a generic structure to power current traffic forecasting models with stronger learning capability to handle aperiodic patterns from traffic series.** DualCast has a dual-branch design to disentangle a traffic observation into two signals: (1) the *intrinsic branch* learns intrinsic (periodic) *spatial-temporal patterns*, and (2) the *environment branch* learns external environment contexts that contain aperiodic patterns. We implement DualCast with three representative traffic forecasting models, that is, STTN [Xu *et al.*, 2020], GMAN [Zheng *et al.*, 2020] and PDFormer [Jiang *et al.*, 2023a], due to their reported strong learning outcomes.

The success of our dual-branch framework relies on three loss functions: *filter loss*, *environment loss*, and *DBI loss*. These functions guide DualCast to disentangle the two types of signals and later fuse the learning outcomes to generate the forecasting results.

(1) The **filter loss** computes the reciprocal of Kullback-Leibler (KL) divergence between the feature representations learned from two branches, ensuring that each branch captures distinct signals from the input. (2) The **environment loss** is designed for the environment branch. It computes the

reciprocal of KL divergence between a batch of training samples and a randomly permuted sequence of those samples in the same batch. This loss encourages DualCast to learn *the diverse environment contexts* at different times, as the samples of the training pair used in the KL divergence are drawn from different periods. (3) The **DBI loss** is designed for the intrinsic branch. It encourages DualCast to learn more separated representations for training samples with different (periodic) traffic patterns while closer representations for samples within the same traffic patterns.

The three models [Xu *et al.*, 2020; Zheng *et al.*, 2020; Jiang *et al.*, 2023a] with which DualCast is implemented all use self-attention. To enhance **their self-attention modules to capture spatial-temporal correlations**, we identify two issues: (1) Existing self-attention-based models [Xu *et al.*, 2020; Zheng *et al.*, 2020; Jiang *et al.*, 2023a] learn spatial and temporal patterns separately, focusing on nodes at the same time step or the same node across time. They neglect correlations between different nodes across time, while such correlations are important for modelling the impact of aperiodic events like the impact of traffic incidents propagating spatially over time. (2) Existing models take either a local attention [Jiang *et al.*, 2023a] or a global attention [Zheng *et al.*, 2020] setup. They compute attention only among connected nodes (based on the adjacency matrix) or among all nodes. This limits receptive fields or loses hierarchical relationships critical for traffic flow propagation.

To address these issues, we propose: (1) a *cross-time attention* module using hierarchical message passing based on a conceptual space-time tree, enabling attention across nodes and time steps to better model spatial-temporal traffic propagation without extra storage or computational overhead. (2) an *attention fusion* module to combine local and global attention, expanding the receptive field and capturing hierarchical node relationships.

Overall, this paper makes the following contributions:

(1) We propose DualCast – a model framework equipped with two branches and three loss functions to disentangle complex traffic observations into two types of signals for more accurate forecasting. DualCast is versatile in terms of the models to form its two branches – we use self-attention-based models for their reported strong learning outcomes.

(2) We propose two enhancements for self-attention-based forecasting models: (i) A cross-time attention module to capture high-order spatial-temporal correlations, and (ii) An attention fusion module to combine global and local attention, enlarging DualCast's receptive field and learning the hierarchical relationships among the nodes.

(3) We conduct experiments on both freeway and urban traffic datasets, integrating DualCast with three self-attention-based models GMAN, STTN, and PDFormer. The results show that: (i) DualCast consistently reduces the forecasting errors for these models, with stronger improvements at times with more complex environment contexts and by up to 9.6% in terms of RMSE; (ii) DualCast also outperforms the SOTA model consistently and by up to 2.6%. Our source code is available at https://github.com/suzy0223/DualCast.

2 Related Work

Traffic forecasting typically employs sequence models [Box *et al.*, 2015; Hochreiter and Schmidhuber, 1997; Wu *et al.*, 2019] to capture temporal patterns and GNNs for spatial correlations [Tian and Pan, 2015; Kumar and Vanajakshi, 2015; Zhao *et al.*, 2017; Yu *et al.*, 2018; Jin *et al.*, 2022; Zheng *et al.*, 2023; Ma *et al.*, 2024; Su *et al.*, 2024b]. Spatial and temporal layers can be arranged sequentially or in parallel, and fused via methods such as gated fusion [Arevalo *et al.*, 2017]. Some GNN-based models [Zhao *et al.*, 2023] connect graph snapshots over time to reduce the negative impact of the ripple effect, which still overlooks time-varying relationships. Self-attention based traffic forecasting models handle this issue easily [Liu *et al.*, 2023; Li *et al.*, 2024].

Moreover, some studies disentangle traffic series into periodic components [Chen *et al.*, 2021; Deng *et al.*, 2021; Fang *et al.*, 2023; Qin *et al.*, 2024; Sun *et al.*, 2024; Yi *et al.*, 2024], different levels [Chang *et al.*, 2024], or invariant and environment signals [Xia *et al.*, 2023; Zhou *et al.*, 2023]. Others adopt memory augmentation to enhance sensitivity to aperiodic signals [Wang *et al.*, 2022; Jiang *et al.*, 2023b]. Our proposed DualCast employs a dual-branch structure with three loss functions and cross-time attention to flexibly capture diverse, aperiodic patterns and environment contexts without relying on predefined patterns. A full discussion is provided in Appendix A of our online technical report [Su *et al.*, 2024a].

3 Preliminaries

Traffic forecasting. We model a network of traffic sensors as a graph $G = (V, E, \mathbf{A})$, where V denotes a set of N nodes (each representing a sensor) and E denotes a set of edges representing the spatial connectivity between the sensors based on the underlying road network. $\mathbf{A} \in \mathbb{R}^{N \times N}$ is an adjacency matrix derived from the graph. If $v_i, v_j \in V$ and $(v_i, v_j) \in E$, then $\mathbf{A}_{i,j} = 1$; otherwise, $\mathbf{A}_{i,j} = 0$.

For each sensor (i.e., a *node* hereafter, for consistency) $v_i \in V$, we use $x_{i,t} \in \mathbb{R}^C$ to represent the traffic observation of v_i at time step t, where C is the number of types of observations, e.g., traffic flow and traffic speed. Further, $\mathbf{X}_t = [x_{1,t}, x_{2,t} \ldots, x_{N,t}] \in \mathbb{R}^{N \times C}$ denotes the observations of all nodes in G at time step t, while $\hat{\mathbf{X}}_t \in \mathbb{R}^{N \times C}$ denotes the forecasts of the nodes in G at time step t. We use $\mathbf{X}_{t_i:t_j}$ to denote the consecutive observations from t_i to t_j.

Problem statement. Given a sensor graph $G = (V, E, \mathbf{A})$, a traffic forecasting model generally adopts an encoder-decoder structure to learn from the traffic observations of the previous T steps and generate forecasts for the following T' steps $\hat{\mathbf{X}}_{t+1:t+T'} = g_\omega(f_\theta(\mathbf{X}_{t-T+1:t}))$, where f_θ and g_ω denote the encoder and the decoder, respectively, and $\theta \in \Theta$ and $\omega \in \Omega$ denote the learnable parameters. We aim to find f_θ and g_ω to minimise the errors between the ground-truth observations and the forecasts:

$$\underset{\theta \in \Theta,\ \omega \in \Omega}{\arg\min} \underset{t \in \mathcal{T}}{\mathbb{E}} \left|\left| g_\omega\big(f_\theta(\mathbf{X}_{t-T+1:t})\big) - \mathbf{X}_{t+1:t+T'} \right|\right|_p, \quad (1)$$

where $\mathcal{T}$ denotes the time range of traffic observations of the dataset, and p is commonly set as 1 or 2.

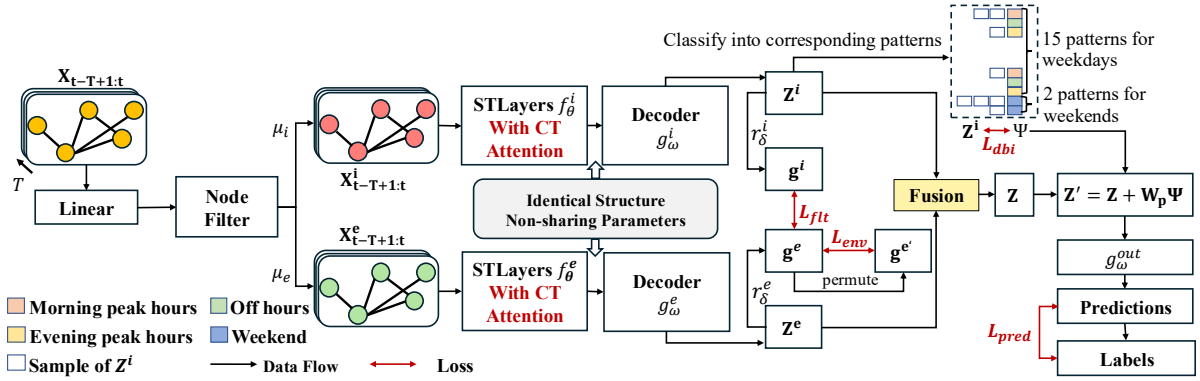

Figure 2: The DualCast framework. DualCast maps the input traffic observations $\mathbf{X}_{t-T+1:t}$ ($\mathbf{X}$, for simplicity) into a D-dimensional space and uses a node filter to disentangle them into intrinsic signals ($\mathbf{X}^i$) and environment signals ($\mathbf{X}^e$). Each signal is fed into a separate branch (intrinsic or environment branch) formed by an encoder (STLayers with CT attention), a decoder, and a function generating traffic representation $\mathbf{Z^i}$ ($\mathbf{Z^e}$) and graph representation $\mathbf{g}^i$ ($\mathbf{g}^e$). Three loss functions are designed to optimise DualCast: (1) Filter loss computes KL divergence between $\mathbf{g}^i$ and $\mathbf{g}^e$ to guide each branch to capture distinct signals from the input. (2) The environment loss computes KL divergence between $\mathbf{g}^e$ and $permute(\mathbf{g}^e)$ to encourage DualCast to learn different environment contexts for different times, and (3) The DBI loss promotes learning distinctive representations for different periodic traffic patterns. DualCast finally fuses $\mathbf{Z^i}$, $\mathbf{Z^e}$, and Ψ to produce $\mathbf{Z}'$, which is then mapped into the output space and compared with the ground truth to compute the prediction loss.

We propose a model optimisation framework named DualCast compatible with recent self-attention-based (*STF* hereafter) models [Xu *et al.*, 2020; Zheng *et al.*, 2020; Jiang *et al.*, 2023a]. Due to space limit, we detail these models in our technical report [Su *et al.*, 2024a] (Appendix B).

4 The DualCast Framework

Fig. 2 shows our proposed DualCast with a *dual branch* structure (Section 4.1), which disentangles traffic observations into two types of underlying signals, namely *intrinsic (periodic) signals* and *environmental (aperiodic) signals* for accurate traffic forecasting. We introduce three loss functions: *filter loss*, *environment loss*, and *DBI loss*, to guide the model to generate distinct representations for these signals.

As self-attention-based traffic forecasting models have competitive performance, we use them as baseline models. We design *rooted sub-tree cross-time attention* (CT attention) module (Section 4.2) which can efficiently capture dynamic and high-order spatial-temporal correlations between sensors on both branches to enhance their performance.

4.1 Dual-branch Structure and Optimisation

Dual-branch structure. The dual-branch structure disentangles the traffic observations into intrinsic and environment signals. The intrinsic branch (IBranch) and environment branch (EBranch) share an identical structure with separate parameters. The intrinsic signals reflect intrinsic (periodic) traffic patterns, while the environment signals reflect external environment (aperiodic) contexts, such as traffic incidents. The two signals together determine the traffic forecasts.

Given a batch of input observations $\mathbf{X} \in \mathbb{R}^{B\times T\times N\times C}$, we compute *disentangling coefficients* μ_i, μ_e for intrinsic and environment signals as $\mu_i, \mu_e = \mathrm{softmax}(\mathrm{Linear}(\mathbf{X}))$, where Linear denotes a linear layer with an output size of 2; Both μ_i and μ_e have shape $\mathbb{R}^{B\times T\times N}$. Then, we produce the intrinsic signals $\mathbf{X}^i = \mu_i \odot \mathbf{X}$ and the environment signals $\mathbf{X}^e = \mu_e \odot \mathbf{X}$, where $\odot$ is element-wise product, and μ_i, μ_e are expanded along the last dimension. These signals are fed into IBranch and EBranch to generate representations $\mathbf{Z^i}$ and $\mathbf{Z^e}$, respectively. The process is detailed for IBranch, with EBranch operating similarly.

In IBranch, $\mathbf{X}^i$ is fed into the spatial-temporal encoder f_θ^i to produce a hidden representation $\mathbf{H}^i$, which is passed to the decoder g_ω^i to produce the output representation of the branch, $\mathbf{Z^i} \in R^{B\times T\times N\times D}$. We concatenate the outputs of both branches to obtain $\mathbf{Z} = \mathrm{Concat}(\mathbf{Z^i}, \mathbf{Z^e})$ and generate the forecasts $\hat{\mathbf{X}}$ from $\mathbf{Z}$ through another linear layer g_ω^{out}.

Model training. We train DualCast using three loss functions: (1) filter loss to separate branch feature spaces, (2) environment loss to learn the impact of environment contexts, and (3) DBI loss to learn different periodic patterns.

Filter loss. Denoted as L_{flt}, is based on KL divergence. It encourages each branch to capture distinct signals. We aggregate the output $\mathbf{Z}^i$ from IBranch along the time dimension by a linear layer and then along node with mean pooling to produce an overall representation $\mathbf{g}^i \in \mathbb{R}^{B\times D}$ of each input sample. This process is denoted as r_δ^i, where δ refers to linear layer parameters. Similarly, we obtain $\mathbf{g}^e$ through r_δ^e from EBranch. We use $\mathrm{softmax}(\cdot)$ to map $\mathbf{g}^e$ and $\mathbf{g}^i$ into distribution and compute the filter loss as follows:

$$L_{flt} = \mathrm{KL}(\mathbf{g}^{\mathrm{i}}, \mathbf{g}^{\mathrm{e}})^{-1}. \tag{2}$$

Environment loss. Denoted as L_{env}, guides the EBranch to learn external environment signals (aperiodic events). Our intuition is that the environment context of different samples from different time periods should be random and hence different (otherwise this becomes a periodic signal). To capture such varying environment contexts, the environment loss guides different samples to generate different environment representations. We randomly permute $\mathbf{g}^e$ along the batch dimension to obtain $\mathbf{g}^{e'} = \pi(\mathbf{g}^{\mathrm{e}})$. We then obtain B sample pairs $(\mathbf{g}_i^e, \mathbf{g}_i^{e'})$, $i \in [1, B]$. We use $\mathrm{softmax}(\cdot)$ to map $\mathbf{g}^e$

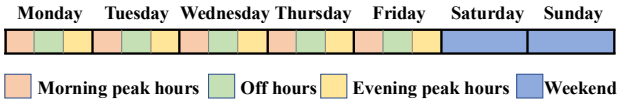

Figure 3: Periodic patterns for the intrinsic branch.

and $\mathbf{g}^{e'}$. We aim to separate the representations of the sample pairs to guide DualCast to generate diverse environment representations for different times. Thus:

$$L_{env} = \mathrm{KL}\big(\pi(\mathbf{g}^{\mathrm{e}}), \mathbf{g}^{\mathrm{e}}\big)^{-1}. \tag{3}$$

DBI loss. Denoted as L_{dbi} and inspired by the Davies–Bouldin index (DBI) [Davies and Bouldin, 1979], guides IBranch to learn representative intrinsic patterns. Traffic observations exhibit different periodic patterns based on time (e.g., workdays vs. weekends, and peak hours vs. off hours). We define 17 time-based patterns (Fig. 3): 15 for workdays (morning peak, off-hour, and evening peak for each weekday), one for Saturdays, and one for Sundays, due to the reduced variation on weekends [Jin *et al.*, 2023; Dey *et al.*, 2023]. Public holidays are treated as Sundays. The output $\mathbf{Z^i}$ of IBranch contains B samples. We classify each sample based on its start time into one of the 17 patterns. This gives a set of sample representations for each pattern. Let P denote the set of 17 patterns, and $p \in P$ refer to one such set. We define a matrix $\Psi \in \mathbb{R}^{|P|\times T\times N\times D}$ as the prototype for 17 patterns and optimise Ψ during training. The intuition of Ψ is that each of 17 patterns may consist of T distinct sub-patterns for each node, with each sub-pattern represented as a D-dimensional vector. The DBI loss guides DualCast to learn more separated representations for the training samples with different periodic patterns, and closer representations for those with the same periodic patterns. We first compute two metrics $\mathcal{S}$ and $\mathcal{P}$ that evaluate the compactness of a pattern and the separation among patterns, respectively.

$$\mathcal{S}_p(\mathbf{Z}^i, \Psi_p) = \frac{1}{|p|}\sum_{\mathbf{Z}^i_j \in p} ||\Psi_p - \mathbf{Z}^i_j||_2. \tag{4}$$

Here, p is an element (also a set) of set P, j is the j-th sample in $\mathbf{Z^i}$, and Ψ_p denotes the slicing of Ψ along the dimension of number of patterns that corresponds to p. Next, we compute $\mathcal{P}_{p,q}$ to evaluate the separation between sets $p, q \in P$, $\mathcal{P}_{p,q} = ||\Psi_p - \Psi_q||_2$. Another metric $\mathcal{R}_{p,q}$ balances the compactness of the two sets and the separation between them:

$$\mathcal{R}_{p,q}(\mathbf{Z^i}, \Psi) = (\mathcal{S}_p + \mathcal{S}_q)\mathcal{P}^{-1}_{p,q}. \tag{5}$$

Based on $\mathcal{R}_{p,q}(\mathbf{Z^i}, \Psi)$, we obtain a quality (in terms of compactness and separation) score of set p, denoted by $\mathcal{D}_p$:

$$\mathcal{D}_p(\mathbf{Z^i}, \Psi) = max_{p\neq q}\mathcal{R}_{p,q}. \tag{6}$$

Finally, we can compute the DBI loss:

$$L_{dbi} = \frac{1}{|P|}\sum_{p\in P}\mathcal{D}_p(\mathbf{Z^i}, \Psi) = \frac{1}{|P|}\sum_{p\in P}\mathcal{D}_p(g^i_\omega(f^i_\theta(\mathbf{X^i})), \Psi). \tag{7}$$

Based on the DBI loss, we can optimise prototype representations for each periodic pattern. We enhance the representation $\mathbf{Z} = \mathrm{Concat}(\mathbf{Z^i}, \mathbf{Z^e})$ by aggregating Ψ as follows:

$$\mathbf{Z}' = \mathbf{Z} + \mathbf{W}\Psi. \tag{8}$$

Here, $\mathbf{W} \in \mathbb{R}^{B\times|P|}$ is a matrix where each row contains a one-hot vector indicating the pattern set to which each sample belongs, i.e., $w_{j,p} = 1$ if $\mathbf{Z^i}_j \in p$, otherwise $w_{j,p} = 0$. Based on Eq. 8, we rewrite the prediction loss as follows:

$$L_{pred} = \mathbb{E}(||g^{out}_\omega(\mathbf{Z}') - \mathbf{Y}||_p) \tag{9}$$

Final loss. Our final loss combines the three loss terms above with the prediction loss (Eq. 9), weighted by hyperparameters α, β, and γ:

$$L = L_{pred} + \alpha L_{flt} + \beta L_{env} + \gamma L_{dbi}. \tag{10}$$

We include model time complexity in Appendix B.2 [Su *et al.*, 2024a].

4.2 Rooted Sub-tree Cross-time Attention

The rooted sub-tree cross-time attention module consists of global and local attention mechanisms, which jointly capture high-order and dynamic spatial-temporal dependencies by learning correlations across time. This module is applied only within the spatial layers. For brevity, we omit the superscript 'sp' in the notation. At each spatial layer, the input $\mathbf{H}^{l-1}_t$ (with $\mathbf{H}^0_t = \mathbf{X}_t$) is first projected into three subspaces to obtain the query $\mathbf{Q}^l$, key $\mathbf{K}^l$, and value $\mathbf{V}^l$. These representations are then used to compute the output $\mathbf{H}^l$. For simplicity, we omit the superscript 'l' in the following notation.

Computing cross-time attention adds nodes from other time steps to the graph G_t has $O(T^2N^2)$ time complexity when using scaled dot products as in prior models (detailed in Appendix B [Su *et al.*, 2024a]). To reduce time complexity in cross-time attention, we first use a *feature mapping function* [Huang *et al.*, 2023]:

$$\mathbf{h}_{t,n} = \frac{\phi(\mathbf{Q}_{t,n})\sum^N_{m=1}(\mathbf{M}_{n,m}\phi(\mathbf{K}_{t,m}))^T\mathbf{V}_{t,m}}{\phi(\mathbf{Q}_{t,n})\sum^N_{m=1}\mathbf{M}_{n,m}\phi(\mathbf{K}_{t,m})^T}, \tag{11}$$

where ϕ denotes a ReLU activation function; n and m are nodes in the graph; and $\mathbf{M}$ represents the connection (edge) between them. The two summations terms $\sum^N_{m=1}\mathbf{M}_{n,m}\phi(\mathbf{K}_{t,m})^T$ and $\sum^N_{m=1}(\mathbf{M}_{n,m}\phi(\mathbf{K}_{t,m}))^T\mathbf{V}_{t,m}$ are shared by all nodes, which are computed once. Thus, we reduce the time complexity.

Global attention. We apply Eq. 11 to compute the self-attention among all nodes at time t, obtaining N vectors $\mathbf{h}_{t,n}$ ($n \in [1, N]$), which form a global attention matrix $\mathbf{H}^{glo}_t$. As Fig. 4(c) shows, the global attention computes attention coefficients between all nodes (i.e., $\mathbf{M}$ in Eq. 11 is a matrix of 1's). We then update the representations of nodes by aggregating those from all other nodes, weighted by the attention coefficients. The time complexity of this process is $O(TN)$.

Local attention. The local attention captures high-level correlations between nodes within a local area across different times. We achieve this goal by constructing an elaborate graph, where nodes from different times are connected. To learn high-level correlations, we reuse the feature mapping function-enhanced self-attention (Eq. 11), instead of the stacked spatial-temporal GNN layers, for better efficiency and effectiveness.

We use two types of edges to help learn cross-time correlations between nodes. For a series of graph snapshots between

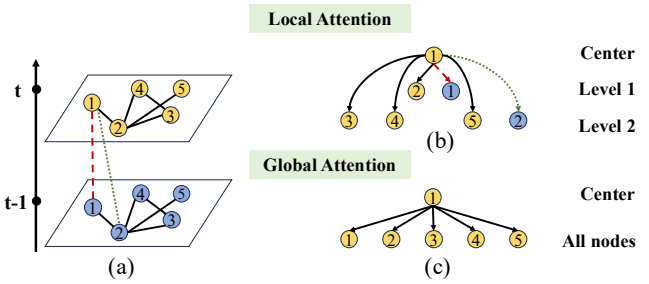

Figure 4: Rooted sub-tree cross-time attention. For simplicity, we set $t' - t'' = 1$. (a) Cross-time attention. Node #1 at time step t serves as the root of the subtree in (b). The red dashed line denotes an edge between observations of Node #1 at different times. The green dotted line denotes an edge between Node #1 and its one-hop neighbour at different times. The black lines denote edges between nodes and their one-hop neighbours observed at a time. (b) The subtree structure is used in local attention. (c) The global attention.

times t' and t'', we construct (1) edges between the same node across different times (red dashed line in Fig. 4(a)), and (2) edges between a node and its one-hop neighbours from other times (green dotted line in Fig. 4(a)). This process yields a large cross-time graph with $N|t'' - t' + 1|$ nodes and edges from the original sensor graph at every time step, and the newly created edges. We use the adjacency matrix of the cross-time graph as $\mathbf{M}$ in Eq. 11, as visualised in Fig. 8 (Appendix B.3 [Su *et al.*, 2024a]), where $\mathbf{A}^k$ is derived from $\mathbf{A}^1$ and k indicates k-hop neighbours.

A simple way to learn high-order relationships from graphs is to apply self-attention Eq. 11, but it ignores the local hierarchical information. For example, the red dashed line and the green dotted line have different traffic propagation patterns and propagation time costs in Fig. 4(a) as a red dashed line only concerns the same node across different times, while a green dotted line concerns nodes at different space and times, which should not be ignored.

To fill this gap, we use a sub-tree structure that decouples the attention into multiple levels, as shown in Fig. 4(b). This structure enables fine-grained control over the contributions from different hops within the graph. In the sub-tree construction process, red dashed lines represent the formation of 1-hop neighbours, while green dotted lines denote 2-hop neighbours. At each level k ($k \in [1, \mathcal{K}]$, where $\mathcal{K}$ denotes the number of levels), we compute the attention weights among the neighbours of a node n. These neighbours' representations are aggregated to obtain the localised representation $\mathbf{h}_{t,n}^{k,loc}$, as formalised in Eq. 12. After computing $\mathbf{h}_{t,n}^{k,loc}$ for all nodes, the resulting vectors are assembled into the matrix $\mathbf{H}_t^{k,loc}$. Subsequently, we aggregate representations from all levels to form the final local attention $\mathbf{H}_t^{loc} = \sum_{k=0}^{\mathcal{K}} w_k \mathbf{H}_t^{k,loc}$. Here, w_k is a learnable parameter to control the contribution of each hop. This computation process can be seen as a k-hop message-passing process. Based on the k-hop message-passing process, the mask $\mathbf{M}^k$ in each step equals to $\mathbf{A}^1$, denoted as $\mathbf{A}$. Fig. 8(b) shows this matrix, where I_N denotes an identity matrix of size N. Since the message-passing process runs for each edge and among all nodes, we obtain $\mathbf{H}_t^{loc}$ with time complexity $O(|E'|)$. Here, E' represents the number of edges after we build the edges across graphs from different time steps (i.e., number of 1's in $\mathbf{A}$).

$$\mathbf{h}_{t,n}^{0,loc} = \mathbf{V}_{t,n},$$

$$\mathbf{h}_{t,n}^{k,loc} = \frac{\phi(\mathbf{Q}_{t,n}) \sum_{m=1}^{N} (\mathbf{M}_{n,m}^k \phi(\mathbf{K}_{t,m}))^T \mathbf{V}_{t,m}}{\phi(\mathbf{Q}_{t,n}) \sum_{m=1}^{N} \mathbf{M}_{n,m}^k \phi(\mathbf{K}_{t,m})^T}. \tag{12}$$

After obtaining $\mathbf{H}_t^{loc}$ and $\mathbf{H}_t^{glo}$, we fuse them as follows:

$$\mathbf{H}_t = \mathbf{H}_t^{loc} + w_{glo} \mathbf{H}_t^{glo}, \tag{13}$$

where w_{glo} is a learnable parameter. Then, we concatenate $\mathbf{H}_t$ from each time step t to obtain the output of the spatial self-attention layer $\mathbf{H} = ||_{t=0}^{T} \mathbf{H}_t$.

We also use a temporal self-attention module to capture the temporal features from the full input time window. We merge $\mathbf{H}^{sp}$ with $\mathbf{H}^{te}$ to obtain the final output of each layer.

Discussion. The high-order and dynamic spatial-temporal relationships play an important role in traffic forecasting. Previous graph-based methods [Li and Zhu, 2021; Song *et al.*, 2020] stack GNNs to capture such correlations, with sub-optimal effectiveness, while the vanilla self-attention models suffer in their quadratic time complexity. Our work addresses these issues and presents a versatile self-attention-based method to exploit the high-order and dynamic spatial-temporal relationships effectively and efficiently.

5 Experiments

5.1 Experimental Setup

Datasets. We use two freeway traffic datasets and an urban traffic dataset: **PEMS03** and **PEMS08** [PeMS, 2001] contain traffic flow data collected by 358 and 170 sensors on freeways in California; **Melbourne** [Su *et al.*, 2024b] contains traffic flow data collected by 182 sensors in the City of Melbourne, Australia. The traffic records in PEMS03 and PEMS08 are given at 5-minute intervals (288 intervals per day), while those in Melbourne are given at 15-minute intervals (96 intervals per day). Melbourne has a higher standard deviation and is more challenging. See Table 3 (Appendix C.1 [Su *et al.*, 2024a]) for the dataset statistics.

Following Li *et al.*, we use records from the past hour to forecast for the next hour, i.e., $T = T' = 1\ hour$ in Eq. 1 over all datasets. We split each dataset into training, validation, and testing sets by 7:1:2 along the time axis.

Competitors. DualCast works with spatial-temporal models that follow the described self-attention-based structure. We implement DualCast with three such models: **GMAN** [Zheng *et al.*, 2020], **STTN** [Xu *et al.*, 2020], and **PDFormer** [Jiang *et al.*, 2023a], denoted as **DualCast-G**, **DualCast-S**, and **DualCast-P**, respectively. We compare with the vanilla GMAN, STTN, and PDFormer models, plus GNN-based models **GWNet** [Wu *et al.*, 2019], **MTGNN** [Wu *et al.*, 2020], and **STPGNN** [Kong *et al.*, 2024]. We further compare DualCast with **MegaCRN** [Jiang *et al.*, 2023b] and **EAST-Net** [Wang *et al.*, 2022], which focus on modelling non-stationarity in spatial-temporal series. We also compare with **STWave** [Fang *et al.*, 2023] and **STNorm** [Deng *et al.*, 2021], which consider disentanglement in forecasting.

Model	PEMS03		PEMS08		Melbourne	
	RMSE↓	MAE↓	RMSE↓	MAE↓	RMSE↓	MAE↓
GWNet	26.420±0.839	15.404±0.052	25.796±0.318	16.314±0.230	25.778±0.136	13.410±0.065
MTGNN	25.413±0.201	14.707±0.070	23.794±0.073	14.898±0.066	25.364±0.291	13.310±0.137
STPGNN	25.889±0.718	14.868±0.141	23.374±0.088	14.202±0.085	25.170±0.083	13.075±0.071
MegaCRN	25.645±0.119	14.733±0.031	24.052±0.333	15.118±0.034	24.482±0.143	12.647±0.033
EASTNet	26.920±1.732	16.356±1.511	27.166±2.088	17.574±1.910	28.494±1.143	15.310±0.746
STNorm	27.328±0.437	16.382±0.191	26.026±0.119	17.090±0.113	25.744±0.277	13.724±0.134
STWave	26.346±0.174	14.975±0.086	23.270±0.108	13.480±0.089	26.918±0.455	14.060±0.341
STTN	27.166±0.408	15.490±0.115	24.984±0.248	15.924±0.200	26.402±0.247	13.790±0.117
GMAN	26.624±0.503	15.520±0.111	23.750±0.194	14.080±0.036	24.496±0.351	12.652±0.136
PDFormer	25.950±0.421	14.690±0.080	23.250±0.099	13.654±0.337	27.072±0.301	14.230±0.069
DualCast-S (ours)	26.282±0.128 (+3.3%)	15.370 ±0.086 (+0.8%)	24.526±0.116 (+1.8%)	15.550±0.119 (+2.3%)	25.474 ±0.184 (+3.5%)	13.316±0.061 (+3.4%)
DualCast-G (ours)	25.582±0.414(+3.9%)	15.094±0.099 (+2.7%)	23.564±0.133 (+0.8%)	13.938±0.114 (+1.0%)	**23.978**±0.105 (+2.1%)	**12.420**±0.057 (+1.8%)
DualCast-P (ours)	**24.898**±0.663 (+4.1%)	**14.666**±0.087 (+0.2%)	**22.998**±0.161 (+1.1%)	**13.332**±0.059 (+2.4%)	26.040±0.150 (+3.8%)	13.542±0.003 (+4.8%)
Error reduction	2.0%	0.2%	1.1%	1.1%	2.1%	1.8%

Table 1: Overall model performance. "↓" indicates lower values are better. The best baseline results are underlined, and the best DualCast results are in boldface. "Error reduction" denotes the percentage decrease in errors of the best DualCast-based model compared to the best baseline. The numbers in blue show error reduction achieved by a DualCast-based model over vanilla models, e.g., DualCast-P vs. PDFormer.

Implementation details. We use the released code of the competitors, except for STTN which is implemented from Libcity [Wang *et al.*, 2021]. We implement DualCast with the self-attention-based models following their source code, using PyTorch. We use the default settings from the source code for both the baseline models and their variants powered by DualCast. We train the models using Adam with a learning rate starting at 0.001, each in 100 epochs. For the models using DualCast, we use grid search on the validation sets to tune the hyper-parameters α, β, and γ. Table 4 (Appendix C.1 [Su *et al.*, 2024a]) lists these hyper-parameter values. All experiments are run on an NVIDIA Tesla A100 GPU with 80 GB RAM. Following Xia *et al.*, we use the average of root mean squared errors (**RMSE**) and mean absolute errors (**MAE**) for evaluation. Results are averaged over five runs.

5.2 Overall Results

Model performance across all times. Table 1 reports forecasting errors averaged over one hour. Powered by DualCast, DualCast-G, DualCast-P, and DualCast-S consistently outperform their vanilla counterparts. DualCast-P has the best performance on freeway traffic datasets PEMS03 and PEMS08, while DualCast-G performs the best on the urban traffic dataset Melbourne. Compared to PEMS03 and PEMS08, Melbourne represents an urban environment with greater variability in the traffic flow series (Table 3). GMAN's simple, robust design explains its strong performance in Melbourne, while PDFormer's reliance on time series clustering excels on PEMS03 and PEMS08 but struggles with Melbourne's variability, hindering cluster formation and accuracy. Fig. 5a further shows the RMSE for forecasting 15, 30, and 60 minutes forecasts, comparing DualCast-G, DualCast-P, and DualCast-S, their vanilla counterparts and top baselines MegaCRN and STPGNN. We see that the DualCast models outperform the baseline models consistently at different forecasting horizons, confirming their effectiveness. We also conducted t-tests and Wilcoxon tests over our model and the best baseline models across all datasets. We find that all results are statistically significant (with $p \ll 10^{-8}$).

Model performance during hours prone to traffic accidents. To verify DualCast's ability to learn complex environment contexts, we examine forecasting results during *complex times* (4:00 pm to 8:00 pm on workdays), which has reported a higher chance of traffic accidents [Karacasu *et al.*, 2011; Ruikar, 2013]. Table 2 shows the results, where "all" means the RMSE at the 1-hour horizon for all days and "cpx" means that at complex times.

All models, including ours, have larger errors at complex times in most cases (except for STWave, GMAN, DualCast-G, and DualCast-P on Melbourne), confirming it as a challenging period. Importantly, the errors of the DualCast-based models increase less at complex times compared to their vanilla counterparts. For example, the error gaps between DualCast-G and GMAN, and DualCast-P and PDFormer on PEMS08 double from 1.6% to 3.0% and 0.7% to 1.4%, respectively. Meanwhile, DualCast-P reduces the errors by up to 9.6% in Melbourne. These results confirm that disentangling intrinsic and environmental contexts improves forecast accuracy. Exceptions on Melbourne may arise due to its high data complexity, variance and skewness, making even a less complex time challenging.

5.3 Ablation Study

We implement six model variants: **w/o-ct** disables the CT attention from DualCast; **w/o-f**, **w/o-dbi**, and **w/o-env** remove the filter loss, the DBI loss, and the environment loss, respectively; **w/o-glo** and **w/o-loc** remove the global attention and local attention (including the CT attention), respectively.

As Fig. 5b shows, all DualCast modules enhance model performance. The DBI loss is more important on PEMS03, as PEMS03's freeway data exhibits clearer patterns across times and days, which DualCast can effectively learn with DBI loss guidance. More results are in Appendix C [Su *et al.*, 2024a].

5.4 Parameter and Case study

Parameter study. We study the impact of α, β, and γ in our loss function (Eq. 10). Results confirm that DualCast is robust without the need for heavy tuning. More details are in Appendix C [Su *et al.*, 2024a].

Case study. We conduct two case studies below.

Responding to traffic accidents. Cross-referencing Melbourne car crash reports [Victoria Road Crash Data, 2023] with the dataset revealed one accident during the data period. Fig. 5(c) compares 15-minute-ahead forecasts from

Model	PEMS03		PEMS08		Melbourne	
	all	cpx	all	cpx	all	cpx
GWNet	30.152	37.276	29.162	31.986	27.766	29.186
MTGNN	27.984	34.842	26.253	28.616	27.264	27.994
STPGNN	29.405	35.346	26.095	27.320	27.018	27.510
MegaCRN	28.472	35.692	27.110	27.442	26.360	26.654
EASTNet	30.434	37.786	31.066	32.674	31.240	33.220
ST-Norm	30.895	38.956	29.366	31.948	27.752	29.304
STWave	29.210	37.312	25.600	27.130	29.562	29.324
STTN	30.386	40.990	28.182	31.400	29.108	30.554
GMAN	28.760	36.078	25.632	26.886	26.066	25.045
PDFormer	28.542	35.416	25.468	27.022	30.048	30.060
DualCast-S (ours)	29.494 (+2.9%)	39.138 (**+4.5%**)	27.522 (+2.3%)	30.454 (**+3.0%**)	27.256 (**+6.4%**)	28.946 (+5.3%)
DualCast-G (ours)	27.766 (+3.5%)	34.450 (**+4.5%**)	25.464 (+0.7%)	26.506 (**+1.4%**)	**25.468** (+2.3%)	**24.398** (**+2.6%**)
DualCast-P (ours)	**27.542** (+3.5%)	**33.950** (**+4.7%**)	**25.048** (+1.6%)	**26.224** (**+3.0%**)	28.134 (+6.4%)	27.168 (**+9.6%**)
Error reduction	1.6%	2.6%	1.7%	2.5%	2.3%	2.6%

Table 2: Model performance (RMSE at the 1-hour horizon) for "all" times (any time of day) and "cpx" times (4:00 pm to 8:00 pm with complex contexts). Best baseline results are underlined, and DualCast's best results are in boldface. blue numbers show error reduction by DualCast-based models compared to their vanilla counterparts.

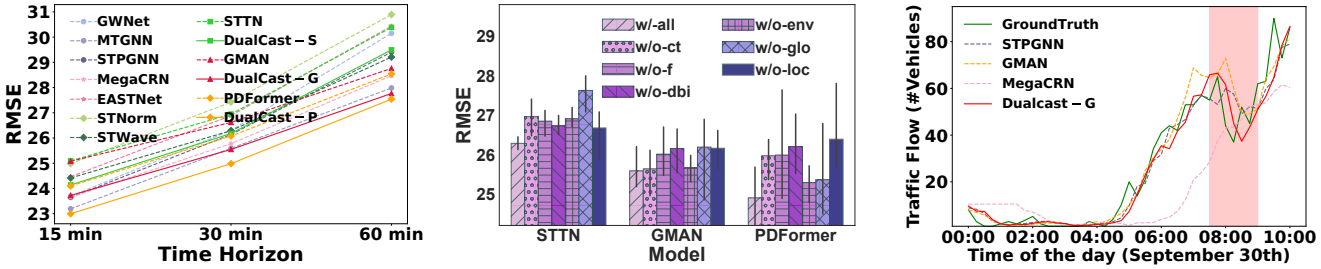

(a) Forecasting error vs. time horizon (b) Ablation Study (c) Car accident

Figure 5: Results on PEMS03 (PEMS08 and Melbourne results in Appendix C.2 to C.4 of our technical report). (a) shows forecasting error vs. time horizon, with dashed lines for baseline models and solid lines for DualCast-based models. The green, red, and orange lines represent DualCast-S, DualCast-G and DualCast-P, respectively, with their counterparts. (b) lists Ablation study results on PEMS03. (c) presents a case study for a car crash at sensor #138 in Melbourne with the occurrence time marked in red.

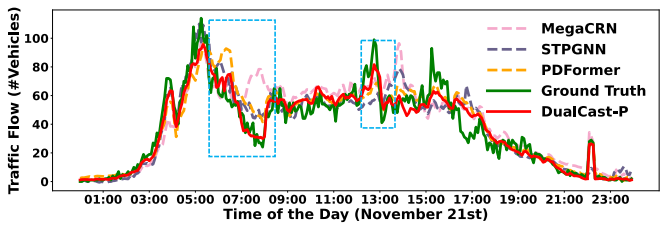

Figure 6: A case study of responding to sudden changes (highlighted in rectangles) in traffic at sensor #97 on PEMS03 on Nov. 21.

DualCast-G (best on this dataset), its vanilla counterpart GMAN, and the top-2 baselines (STPGNN, MegaCRN) at the sensor nearest the accident. Around 8:00, DualCast-G quickly captures the traffic change caused by the crash, producing forecasts closest to the ground truth.

Responding to sudden changes in traffic. On the PEMS datasets, ground-truth traffic events are unavailable. Instead, we found two representative sensors (#72, see Appendix C.4 [Su *et al.*, 2024a] and #97) on PEMS03 with sudden changes on November 21st, 2018. Fig. 6 shows the ground-truth traffic flow and 1-hour-ahead forecasts by MegaCRN, STPGNN, PDFormer, and DualCast-P at Sensor #97. DualCast-P closely aligns with the ground truth, especially during sudden changes, again highlighting the strength of DualCast. More results are in Appendix C [Su *et al.*, 2024a], including PEMS08 and Melbourne results, an analysis of model scalability, effectiveness and potential for GNN-based models, and visualisations for disentangling results.

6 Conclusion

We proposed a framework named DualCast that enhances the robustness of self-attention-based traffic forecasting models, including the SOTA, in handling scenarios with complex environment contexts. DualCast takes a dual-branch structure to disentangle the impact of complex environment contexts, as guided by three loss functions. We further proposed a cross-time attention module to capture high-order spatial-temporal relationships. We performed experiments on real-world freeway and urban traffic datasets, where models powered by DualCast outperform their original versions by up to 9.6%. The best DualCast-based model outperforms the SOTA model by up to 2.6%, in terms of forecasting errors.

Ethical Statement

All datasets used in this study are publicly available and do not contain any personally identifiable information. There are no ethical concerns associated with this work.

Acknowledgments

This work is in part supported by the Australian Research Council (ARC) via Discovery Projects DP230101534 and DP240101006. Jianzhong Qi is supported by ARC Future Fellowship FT240100170. Feng Liu is supported by the ARC with grant numbers DE240101089, LP240100101, DP230101540 and the NSF&CSIRO Responsible AI program with grant number 2303037.

References

[Arevalo *et al.*, 2017] John Arevalo, Thamar Solorio, Manuel Montes-y Gómez, and Fabio A González. Gated Multimodal Units for Information Fusion. *arXiv preprint arXiv:1702.01992*, 2017.

[Box *et al.*, 2015] George E. P. Box, Gwilym M. Jenkins, Gregory C. Reinsel, and Greta M. Ljung. *Time Series Analysis: Forecasting and Control*. John Wiley & Sons, 2015.

[Chang *et al.*, 2024] Ching Chang, Chiao-Tung Chan, Wei-Yao Wang, Wen-Chih Peng, and Tien-Fu Chen. TimeDRL: Disentangled Representation Learning for Multivariate Time-Series. In *ICDE*, 2024.

[Chen *et al.*, 2021] Xinqiang Chen, Huixing Chen, Yongsheng Yang, Huafeng Wu, Wenhui Zhang, Jiansen Zhao, and Yong Xiong. Traffic Flow Prediction by an Ensemble Framework with Data Denoising and Deep Learning Model. *Physica A: Statistical Mechanics and Its Applications*, 2021.

[Davies and Bouldin, 1979] David L Davies and Donald W Bouldin. A Cluster Separation Measure. *IEEE Transactions on Pattern Analysis and Machine Intelligence*, 1979.

[Deng *et al.*, 2021] Jinliang Deng, Xiusi Chen, Renhe Jiang, Xuan Song, and Ivor W Tsang. ST-Norm: Spatial and Temporal Normalization for Multi-variate Time Series Forecasting. In *KDD*, 2021.

[Dey *et al.*, 2023] Subhrasankha Dey, Stephan Winter, Martin Tomko, and Niloy Ganguly. Traffic Count Estimation at Basis Links without Path Flow and Historic Data. *IEEE Transactions on Intelligent Transportation Systems*, 2023.

[Fang *et al.*, 2021] Zheng Fang, Qingqing Long, Guojie Song, and Kunqing Xie. Spatial-Temporal Graph ODE Networks for Traffic Flow Forecasting. In *KDD*, 2021.

[Fang *et al.*, 2023] Yuchen Fang, Yanjun Qin, Haiyong Luo, Fang Zhao, Bingbing Xu, Liang Zeng, and Chenxing Wang. When Spatio-Temporal Meet Wavelets: Disentangled Traffic Forecasting via Efficient Spectral Graph Attention Networks. In *ICDE*, 2023.

[Guo *et al.*, 2019] Shengnan Guo, Youfang Lin, Ning Feng, Chao Song, and Huaiyu Wan. Attention Based Spatial-Temporal Graph Convolutional Networks for Traffic Flow Forecasting. In *AAAI*, 2019.

[Hochreiter and Schmidhuber, 1997] Sepp Hochreiter and Jürgen Schmidhuber. Long Short-Term Memory. *Neural Computation*, 1997.

[Huang *et al.*, 2023] Siyuan Huang, Yunchong Song, Jiayue Zhou, and Zhouhan Lin. Tailoring Self-Attention for Graph via Rooted Subtrees. In *NeurIPS*, 2023.

[Jiang *et al.*, 2023a] Jiawei Jiang, Chengkai Han, Wayne Xin Zhao, and Jingyuan Wang. PDFormer: Propagation Delay-Aware Dynamic Long-Range Transformer for Traffic Flow Prediction. In *AAAI*, 2023.

[Jiang *et al.*, 2023b] Renhe Jiang, Zhaonan Wang, Jiawei Yong, Puneet Jeph, Quanjun Chen, Yasumasa Kobayashi, Xuan Song, Shintaro Fukushima, and Toyotaro Suzumura. Spatio-Temporal Meta-Graph Learning for Traffic Forecasting. In *AAAI*, 2023.

[Jin *et al.*, 2022] Yilun Jin, Kai Chen, and Qiang Yang. Selective Cross-City Transfer Learning for Traffic Prediction via Source City Region Re-Weighting. In *KDD*, 2022.

[Jin *et al.*, 2023] Yilun Jin, Kai Chen, and Qiang Yang. Transferable Graph Structure Learning for Graph-based Traffic Forecasting across Cities. In *KDD*, 2023.

[Karacasu *et al.*, 2011] Murat Karacasu, Arzu Er, Safak Bilgic, and Hasan B Barut. Variations in Traffic Accidents on Seasonal, Monthly, Daily and Hourly Basis: Eskisehir Case. *Procedia-Social and Behavioral Sciences*, 2011.

[Kong *et al.*, 2024] Weiyang Kong, Ziyu Guo, and Yubao Liu. Spatio-Temporal Pivotal Graph Neural Networks for Traffic Flow Forecasting. In *AAAI*, 2024.

[Kumar and Vanajakshi, 2015] S Vasantha Kumar and Lelitha Vanajakshi. Short-Term Traffic Flow Prediction Using Seasonal ARIMA Model with Limited Input Data. *European Transport Research Review*, 2015.

[Li and Zhu, 2021] Mengzhang Li and Zhanxing Zhu. Spatial-Temporal Fusion Graph Neural Networks for Traffic Flow Forecasting. In *AAAI*, 2021.

[Li *et al.*, 2018] Yaguang Li, Rose Yu, Cyrus Shahabi, and Yan Liu. Diffusion Convolutional Recurrent Neural Network: Data-Driven Traffic Forecasting. In *ICLR*, 2018.

[Li *et al.*, 2024] Shuhao Li, Yue Cui, Libin Li, Weidong Yang, Fan Zhang, and Xiaofang Zhou. ST-ABC: Spatio-Temporal Attention-Based Convolutional Network for Multi-Scale Lane-Level Traffic Prediction. In *ICDE*, 2024.

[Liu *et al.*, 2022] Xu Liu, Yuxuan Liang, Chao Huang, Yu Zheng, Bryan Hooi, and Roger Zimmermann. When do Contrastive Learning Signals Help Spatio-temporal Graph Forecasting? In *SIGSPATIAL*, 2022.

[Liu *et al.*, 2023] Hangchen Liu, Zheng Dong, Renhe Jiang, Jiewen Deng, Jinliang Deng, Quanjun Chen, and Xuan Song. Spatio-temporal Adaptive Embedding Makes Vanilla Transformer SOTA For Traffic Forecasting. In *CIKM*, 2023.

[Ma *et al.*, 2024] Minbo Ma, Jilin Hu, Christian S Jensen, Fei Teng, Peng Han, Zhiqiang Xu, and Tianrui Li. Learning Time-aware Graph Structures for Spatially Correlated Time Series Forecasting. In *ICDE*, 2024.

[PeMS, 2001] PeMS. https://pems.dot.ca.gov, 2001.

[Qi *et al.*, 2022] Jianzhong Qi, Zhuowei Zhao, Egemen Tanin, Tingru Cui, Neema Nassir, and Majid Sarvi. A Graph and Attentive Multi-Path Convolutional Network for Traffic Prediction. *IEEE Transactions on Knowledge and Data Engineering*, 2022.

[Qin *et al.*, 2024] Jianyang Qin, Yan Jia, Yongxin Tong, Heyan Chai, Ye Ding, Xuan Wang, Binxing Fang, and Qing Liao. MUSE-Net: Disentangling Multi-Periodicity for Traffic Flow Forecasting. In *ICDE*, 2024.

[Ruikar, 2013] Manisha Ruikar. National Statistics of Road Traffic Accidents in India. *Journal of Orthopaedics, Traumatology and Rehabilitation*, 2013.

[Song *et al.*, 2020] Chao Song, Youfang Lin, Shengnan Guo, and Huaiyu Wan. Spatial-Temporal Synchronous Graph Convolutional Networks: A New Framework for Spatial-Temporal Network Data Forecasting. In *AAAI*, 2020.

[Su *et al.*, 2024a] Xinyu Su, Feng Liu, Yanchuan Chang, Egemen Tanin, Majid Sarvi, and Jianzhong Qi. DualCast: Disentangling Aperiodic Events from Traffic Series with a Dual-Branch Model. *arXiv preprint arXiv:2411.18286*, 2024.

[Su *et al.*, 2024b] Xinyu Su, Jianzhong Qi, Egemen Tanin, Yanchuan Chang, and Majid Sarvi. Spatial-Temporal Forecasting for Regions without Observations. In *EDBT*, 2024.

[Sun *et al.*, 2024] Ke Sun, Pei Liu, Pengfei Li, and Zhifang Liao. ModWaveMLP: MLP-Based Mode Decomposition and Wavelet Denoising Model to Defeat Complex Structures in Traffic Forecasting. In *AAAI*, 2024.

[Tang *et al.*, 2024] Yujin Tang, Lu Qi, Fei Xie, Xiangtai Li, Chao Ma, and Ming-Hsuan Yang. PredFormer: Transformers Are Effective Spatial-Temporal Predictive Learners. *arXiv preprint arXiv:2410.04733*, 2024.

[Tian and Pan, 2015] Yongxue Tian and Li Pan. Predicting Short-term Traffic Flow by Long Short-term Memory Recurrent Neural Network. In *IEEE International Conference on Smart City/SocialCom/SustainCom*, 2015.

[Victoria Road Crash Data, 2023] Victoria Road Crash Data. https://discover.data.vic.gov.au/dataset/victoria-road-crash-data, 2023.

[Wang *et al.*, 2020] Xiaoyang Wang, Yao Ma, Yiqi Wang, Wei Jin, Xin Wang, Jiliang Tang, Caiyan Jia, and Jian Yu. Traffic Flow Prediction via Spatial Temporal Graph Neural Network. In *WWW*, 2020.

[Wang *et al.*, 2021] Jingyuan Wang, Jiawei Jiang, Wenjun Jiang, Chao Li, and Wayne Xin Zhao. LibCity: An Open Library for Traffic Prediction. In *SIGSPATIAL*, 2021.

[Wang *et al.*, 2022] Zhaonan Wang, Renhe Jiang, Hao Xue, Flora D Salim, Xuan Song, and Ryosuke Shibasaki. Event-aware Multimodal Mobility Nowcasting. In *AAAI*, 2022.

[Wu *et al.*, 2019] Zonghan Wu, Shirui Pan, Guodong Long, Jing Jiang, and Chengqi Zhang. Graph WaveNet for Deep Spatial-Temporal Graph Modeling. In *IJCAI*, 2019.

[Wu *et al.*, 2020] Zonghan Wu, Shirui Pan, Guodong Long, Jing Jiang, Xiaojun Chang, and Chengqi Zhang. Connecting the Dots: Multivariate Time Series Forecasting with Graph Neural Networks. In *KDD*, 2020.

[Xia *et al.*, 2023] Yutong Xia, Yuxuan Liang, Haomin Wen, Xu Liu, Kun Wang, Zhengyang Zhou, and Roger Zimmermann. Deciphering Spatio-Temporal Graph Forecasting: A Causal Lens and Treatment. *NeurIPS*, 2023.

[Xu *et al.*, 2020] Mingxing Xu, Wenrui Dai, Chunmiao Liu, Xing Gao, Weiyao Lin, Guo-Jun Qi, and Hongkai Xiong. Spatial-Temporal Transformer Networks for Traffic Flow Forecasting. *arXiv preprint arXiv:2001.02908*, 2020.

[Yi *et al.*, 2024] Kun Yi, Qi Zhang, Wei Fan, Hui He, Liang Hu, Pengyang Wang, Ning An, Longbing Cao, and Zhendong Niu. FourierGNN: Rethinking Multivariate Time Series Forecasting from a Pure Graph Perspective. In *NeurIPS*, 2024.

[Yu *et al.*, 2018] Bing Yu, Haoteng Yin, and Zhanxing Zhu. Spatio-Temporal Graph Convolutional Networks: A Deep Learning Framework for Traffic Forecasting. In *IJCAI*, 2018.

[Zhao *et al.*, 2017] Zheng Zhao, Weihai Chen, Xingming Wu, Peter CY Chen, and Jingmeng Liu. LSTM Network: A Deep Learning Approach for Short-Term Traffic Forecast. *IET Intelligent Transport Systems*, 2017.

[Zhao *et al.*, 2023] Yusheng Zhao, Xiao Luo, Wei Ju, Chong Chen, Xian-Sheng Hua, and Ming Zhang. Dynamic Hypergraph Structure Learning for Traffic Flow Forecasting. In *ICDE*, 2023.

[Zheng *et al.*, 2020] Chuanpan Zheng, Xiaoliang Fan, Cheng Wang, and Jianzhong Qi. GMAN: A Graph Multi-Attention Network for Traffic Prediction. In *AAAI*, 2020.

[Zheng *et al.*, 2023] Chuanpan Zheng, Xiaoliang Fan, Cheng Wang, Jianzhong Qi, Chaochao Chen, and Longbiao Chen. INCREASE: Inductive Graph Representation Learning for Spatio-Temporal Kriging. In *WWW*, 2023.

[Zhou *et al.*, 2023] Zhengyang Zhou, Qihe Huang, Kuo Yang, Kun Wang, Xu Wang, Yudong Zhang, Yuxuan Liang, and Yang Wang. Maintaining the Status Quo: Capturing Invariant Relations for OOD Spatiotemporal Learning. In *KDD*, 2023.